University of Wollongong

Research Online

Faculty of Engineering and Information Sciences - Papers: Part A

Faculty of Engineering and Information Sciences

1-1-2014

On the efficient channel state information compression and feedback for downlink MIMO-OFDM systems

Yong Ping Zhang
Huawei Technologies Company, yongping.zhang@huawei.com

Peng Wang
University of Sydney

Shulan Feng
Huawei Technologies Company

Philipp Zhang
Huawei Technologies Company

Sheng Tong
University of Wollongong, sheng@uow.edu.au

Follow this and additional works at: https://ro.uow.edu.au/eispapers

 Part of the Engineering Commons, and the Science and Technology Studies Commons

Recommended Citation

Zhang, Yong Ping; Wang, Peng; Feng, Shulan; Zhang, Philipp; and Tong, Sheng, "On the efficient channel state information compression and feedback for downlink MIMO-OFDM systems" (2014). *Faculty of Engineering and Information Sciences - Papers: Part A*. 3339.
https://ro.uow.edu.au/eispapers/3339

Research Online is the open access institutional repository for the University of Wollongong. For further information contact the UOW Library: research-pubs@uow.edu.au

On the efficient channel state information compression and feedback for downlink MIMO-OFDM systems

Abstract

This paper is concerned with the efficient compression and feedback of channel state information (CSI) in downlink multiple-input multiple-output (MIMO) orthogonal frequency-division multiplexing (OFDM) systems. Inspired by video coding, we propose a novel CSI compression and feedback scheme, referred to as hybrid transform coding (HTC). HTC consists of two coding types, i.e., selective time-domain coding (STDC) and differential time-domain coding (DTDC), which are adopted to exploit the correlation of CSI in both the frequency and time domains. We first develop closed-form expressions for the overhead-distortion performance of these two coding types in HTC. The parameters involved in HTC are then optimized based on the analytical results. Finally, the system-level performance of HTC is evaluated in both maximum eigenmode beamforming (MEB)-based single-user MIMO (SU-MIMO) and zero-forcing beamforming (ZFBF)-based multiuser MIMO (MU-MIMO) under Long Term Evolution Advanced (LTE-A) Release 10-based cellular networks. Simulation results show that HTC can significantly outperform the available alternative.

Keywords

Channel state information (CSI), hybrid transform coding (HTC), multiple-input multiple-output (MIMO), orthogonal frequency-division multiplexing (OFDM)

Disciplines

Engineering | Science and Technology Studies

Publication Details

Y. Zhang, P. Wang, S. Feng, P. Zhang & S. Tong, "On the efficient channel state information compression and feedback for downlink MIMO-OFDM systems," IEEE Transactions on Vehicular Technology, vol. 63, (7) pp. 3263-3275, 2014.

This journal article is available at Research Online: https://ro.uow.edu.au/eispapers/3339

On the Efficient Channel State Information Compression and Feedback for Downlink MIMO-OFDM Systems

Yong-Ping Zhang, *Member, IEEE,* Peng Wang, *Member, IEEE,* Shulan Feng, *Member, IEEE,* Philipp Zhang, *Member, IEEE,* and Sheng Tong,

***Abstract*—This paper is concerned with the efficient compression and feedback of channel state information (CSI) in downlink multiple-input multiple-output (MIMO) orthogonal frequency division multiplexing (OFDM) systems. Inspired by video coding, we propose a novel CSI compression and feedback scheme, referred to as hybrid transform coding (HTC). HTC consists of two coding types, i.e., selective time-domain coding (STDC) and differential time-domain coding (DTDC), which are adopted to exploit the correlation of CSI in both the frequency and time domains. We first develop closed-form expressions for the overhead-distortion performance of these two coding types in HTC. The parameters involved in HTC are then optimized based on the analytical results. Finally, the system level performance of HTC is evaluated in both maximum eigenmode beamforming (MEB) based single-user MIMO (SU-MIMO) and zeroforcing beamforming (ZFBF) based multi-user MIMO (MU-MIMO) under Long-Term Evolution-Advanced (LTE-A) Release 10 based cellular networks. Simulation results show that HTC can significantly outperform the available alternative.**

***Index Terms*—Channel state information (CSI), multiple-input multiple-output (MIMO), orthogonal frequency division multiplexing (OFDM), hybrid transform coding (HTC).**

I. Introduction

The multiple-input multiple-output (MIMO) technique has been widely studied in the past two decades [1]–[4] due to its capability of significantly improving the system spectrum efficiency. Channel state information (CSI) fed back from user equipments (UEs) plays an important role in downlink MIMO systems operating in the frequency-division duplex (FDD) mode. With CSI at the base station (BS), the system performance can be enhanced by adaptively customizing the transmitted waveforms to the channel, enabling channel-aware scheduling for multiple UEs, and so on. However, in practical wireless environments, the feedback link capacity is always limited. The infinite feedback of CSI to the BS is generally impossible. Hence the overhead of the feedback CSI that guarantees an acceptable CSI accuracy at the BS is always a serious concern.

Recently, a family of CSI compression schemes based on directional quantization have been intensively investigated [4], [5]. The directions of the channel vectors are recognized as the most important information and are quantized by a vector quantization codebook consisting of unit vectors distributed on a multi-dimensional complex sphere. In [6], accurate bounds on the achievable ergodic rate of a zero-forcing beamforming (ZFBF) based system with directional quantization are derived.

The abovementioned research efforts only focus on the CSI compression in frequency flat fading channels. As a fundamental technique for the high speed wireless transmission, orthogonal frequency division multiplexing (OFDM) has been adopted for transmission over frequency selective channels in current and next generation wireless standards such as IEEE 802.16 [7] and Long-Term Evolution-Advanced (LTE-A) [8]. In [9], a time-domain coding (TDC) scheme is proposed for CSI compression of OFDM systems over frequency selective channels. This scheme achieves satisfactory performance by exploiting the correlation among different sub-carriers. However, it does not take any advantage of the channel correlation in the time domain.

Enlightened by TDC, we develop a novel CSI compression and feedback scheme, referred to as hybrid transform coding (HTC) in this paper, for downlink MIMO-OFDM systems. HTC consists of two coding types, i.e., selective time-domain coding (STDC) and differential time-domain coding (DTDC). These two coding types follow the idea of TDC and compress the CSI in the time domain directly so as to take full advantage of the CSI correlation in the frequency domain. The key feature distinguishing them from TDC is that they induce less overhead by selecting only a part of most significant taps for compression. In addition, DTDC can further exploit the CSI correlation in the time domain by only compressing the difference between adjacent available CSI. The corresponding compression efficiency could be very high in the low velocity scenario. We first derive the closed-form expressions for the overhead-distortion performance of each coding type, based on which the parameter settings of HTC are optimized. Finally, the validity of HTC in real-world wireless environments with practical settings (such as UE selection, feedback delay and

Copyright (c) 2013 IEEE. Personal use of this material is permitted. However, permission to use this material for any other purposes must be obtained from the IEEE by sending a request to pubs-permissions@ieee.org. This work was partly supported by NSFC Grand 61001130.

The material in this paper was presented in part at the IEEE International Conference on Communications (ICC), Kyoto, Japan, June, 2011.

Yong-Ping Zhang and Shulan Feng are with the Research Department of Hisilicon, Huawei Technologies Co., Ltd, Beijing, P. R. China (e-mail: yongping.zhang@huawei.com; shulan.feng@huawei.com).

Peng Wang is with the School of Electrical and Information Engineering, the University of Sydney, Sydney, Australia (e-mail: peng.wang@sydney.edu.au).

Philipp Zhang is with the Research Department of Hisilicon, Huawei Technologies Co., Ltd, Plano, Texas, USA (e-mail: philipp.zhang@huawei.com).

Sheng Tong is with the School of Electrical, Computer and Telecommunications Engineering, University of Wollongong, NSW, Australia (email: sheng@uow.edu.au).

hybrid automatic repeat request (HARQ)) is verified by system level simulations based on LTE-A Release 10. Numerical results show that HTC significantly outperforms the available alternative.

II. System Model

Consider a downlink MIMO-OFDM system containing one N-antenna BS and M single-antenna UEs. In the time domain, the channel is modelled to be block fading, i.e., the channel remains unchanged within each block and varies from block to block. This time-domain channel can be converted into a set of K parallel subcarriers in the frequency domain via discrete Fourier transform (DFT). More specifically, at the s-th block, the CSI for the links from the BS to UE m ($m = 0, 1, \cdots, M-1$), which is assumed perfectly known at UE m, is given by

$$\boldsymbol{H}_m^{(s)} = \begin{bmatrix} H_m^{(s)}(0,0) & \cdots & H_m^{(s)}(0,N-1) \\ \vdots & \ddots & \vdots \\ H_m^{(s)}(K-1,0) & \cdots & H_m^{(s)}(K-1,N-1) \end{bmatrix} \quad (1)$$

where each entry, $H_m^{(s)}(k,n)$ $(k = 0, \cdots, K-1, n = 0, \cdots, N-1)$, represents the CSI for the link from the n-th BS antenna to the m-th UE on the k-th subcarrier. Our task in this paper is to find an efficient compression scheme for $\{\boldsymbol{H}_m^{(s)} | \, m = 0, \cdots, M-1\}$ with minor distortion. We will also analyse the overhead-distortion performance of the proposed scheme and examine the corresponding system level performance in real-world wireless environments.

For simplicity, we assume that the CSI for all UEs is independent and identically distributed (i.i.d.). We further assume that, for each UE, the CSI from different BS antennas are also i.i.d., i.e., there is no correlation among BS antennas[1]. Consequently, the compression operations are the same for the CSI across UEs and BS antennas. Hence unless otherwise stated, we omit the subscript m (e.g., $\boldsymbol{H}_m^{(s)}$ is simplified as $\boldsymbol{H}^{(s)}$) from now on without incurring confusion.

By definition, each column of $\boldsymbol{H}^{(s)}$ in (1), denoted by $\boldsymbol{H}^{(s)}(\cdot, n)$, represents the frequency-domain CSI for the link corresponding to the n-th BS antenna, which is transformed from the time-domain CSI via DFT, i.e.,

$$\boldsymbol{H}^{(s)}(\cdot, n) = \boldsymbol{F} \cdot \boldsymbol{h}^{(s)}(n) \quad (2)$$

where $\boldsymbol{F} = \{f_{a,b}\}_{K \times K}$ is a K-by-K DFT matrix with $f_{a,b} = e^{-j2\pi ab/K}$, and the time-domain CSI

$$\boldsymbol{h}^{(s)}(n) = [h^{(s)}(0,n), h^{(s)}(1,n), \cdots, h^{(s)}(K-1,n)]^T \quad (3)$$

consists of K entries (referred to as 'taps' conventionally) that are modelled to be equally spaced in the time domain with gap Δt. Specifically, each entry in $\boldsymbol{h}^{(s)}(n)$, i.e., $h^{(s)}(k,n)$, denotes the channel coefficient of the k-th tap with time delay $(k-1)\Delta t$. These taps with different time delays are caused by the multi-path effect of the channel. In practice, $\boldsymbol{h}^{(s)}(n)$ always contains a small number (denoted by L below) of non-zero taps with their delay indexes denoted by $\{k^{(l)} | \, l = 0, 1, \cdots, L-1\}$. These non-zero taps are commonly assumed to be mutually independent, complex Gaussian random variables with zero means and power delay profile [11] $(\sigma_0^2, \sigma_1^2, \cdots, \sigma_{L-1}^2)$ where

$$\sigma_l^2 \triangleq \mathrm{E}\left(\left|h^{(s)}(k^{(l)}, n)\right|^2\right), \quad l = 0, 1, \cdots, L-1 \quad (4)$$

and $\mathrm{E}(\cdot)$ is the ensemble average operator. Their average total power is assumed to be normalized, i.e., $\sum_{l=0}^{L-1} \sigma_l^2 = 1$. Due to the close placement of antennas at the BS in most wireless systems, we assume that Δt remains the same for all links between the BS and each UE and known at both sides. We further assume that $\{k^{(l)} | \, l = 0, 1, \cdots, L-1\}$ are the same for all the N links of each UE. Note that the above assumptions have been widely adopted in well-known channel models including 3rd Generation Partnership Project (3GPP) spatial channel model (SCM) [14].

The time-domain correlation of the channel can be described by the first-order autoregressive model (AR1) [10]. Under the assumption that the CSI varies every block, we have

$$h^{(s)}(k^{(l)}, n) = \rho \cdot h^{(s-1)}(k^{(l)}, n) + \sqrt{1-\rho^2} \cdot \xi^{(s)}(k^{(l)}, n), \forall n, l \quad (5)$$

where ρ $(0 \le \rho \le 1)$ represents the CSI correlation between the adjacent blocks and the terms of $\xi^{(s)}(k^{(l)}, n)$ and $h^{(s)}(k^{(l)}, n)$ are i.i.d.. Note that the delay indexes of non-zero taps are slow varying and remain unchanged during a period, e.g., τ blocks, where τ is much larger than 1. The total number of non-zero taps is assumed fixed at L for all links.

III. Basic Principles of CSI Compression

In this paper, two basic principles are adopted to exploit the CSI correlation in the frequency and time domains respectively.

Principle 1: The frequency-domain correlation is exploited by compressing the CSI in the time domain.

To exploit the correlation of CSI in the frequency domain during the compression of $\boldsymbol{H}^{(s)}$, a straightforward approach is to sample K^* $(K^* \le K)$ complex entries of each column vector $\boldsymbol{H}^{(s)}(\cdot, n)$ directly. The following theorem gives a lower bound for the minimum value of K^* that guarantees perfect CSI reconstruction. This theorem is the key of the compression scheme developed in this paper, whose proof is given in Appendix A.

Theorem 1: A necessary condition to perfectly reconstruct the CSI from direct frequency-domain sampling is

$$K^* \ge 2L. \quad (6)$$

Theorem 1 indicates that, to guarantee perfect reconstruction for the CSI of each antenna link, the number of variables that need compression in the frequency domain is at least twice of that in the time domain. Comparatively, the CSI concentrates on fewer coefficients in the time domain and can then be compressed more efficiently. This characteristic has been widely utilized in source coding to reduce the statistical

[1]When the BS antennas are correlated with each other due to close deployment, a higher compression efficiency can be achieved by exploiting the correlation in the spatial domain. In this paper, we only focus on how to exploit the correlation in the time and frequency domains. The development of a more efficient compression method to further exploit the correlation in the spatial domain is left as our future work.

correlation [12] and is adopted in this paper to exploit the frequency-domain correlation of CSI.

Principle 2: The time-domain correlation of CSI is exploited by the differential coding method.

As the basic implementation requirement of closed-loop MIMO, the relative velocity between the BS and UE is always very low, implying that ρ in (5) is close to 1. Therefore, the adjacent CSI (either in the time domain or frequency domain) is similar to each other and their difference always has a smaller dynamic range compared with the original coefficients. This indicates that, instead of quantizing the large-scaled channel coefficients directly, we can quantize this small-scaled difference using fine quantization steps to reduce reconstruction error. Hence the compression efficiency is further increased.

IV. Hybrid Transform Coding

Based on the discussion in Section III, we develop a novel compression and feedback scheme referred to as hybrid transform coding (HTC) [13] in this paper. The working flow of HTC is shown in Fig. 1. HTC involves two coding types, i.e., selective time-domain coding and differential time-domain coding. These two coding types and the overall HTC scheme are introduced as follows.

A. Selective Time-Domain Coding (STDC)

With STDC, we first perform K-point inverse DFT (IDFT) on each channel vector $\boldsymbol{H}^{(s)}(\cdot,n)$ and obtain $\boldsymbol{h}^{(s)}(n)$. Among the L non-zero taps $\{h^{(s)}(k^{(l)},n)|\, l=0,1,\cdots,L-1\}$ of each link, we only select L^* $(L^* \le L)$ most significant ones and quantize their real and imaginary parts separately by a common B-bit codebook $Q^0=\{Q_0^0,Q_1^0,\cdots,Q_{2^B-1}^0\}$ that is pre-designed and known at both the UE and the BS. Finally, the quantized indexes of these selected taps are fed back to the BS together with the binary representations of their corresponding delay indexes.

The reconstruction procedure of compressed CSI using STDC at the BS is as follows. Upon receiving the feedback information for the selected L^* taps of each antenna link from the UE, the BS first de-quantizes these tap coefficients based on the codebook Q^0. Combining these tap coefficients and the corresponding recovered delay indexes, we can form the reconstructed time-domain CSI (denoted by $\tilde{\boldsymbol{h}}^{(s)}(n)$). Note that in $\tilde{\boldsymbol{h}}^{(s)}(n)$, except the de-quantized coefficients corresponding to the L^* selected taps, the other coefficients are set to be 0. Finally, DFT is performed on $\tilde{\boldsymbol{h}}^{(s)}(n)$ to obtain the corresponding frequency-domain CSI (denoted by $\tilde{\boldsymbol{H}}^{(s)}(\cdot,n)$).

B. Differential Time-Domain Coding (DTDC)

To compress $\boldsymbol{H}^{(s)}(\cdot,n)$ using DTDC, the UE should have the knowledge of the reconstructed time-domain CSI of the previous OFDM symbol, i.e., $\tilde{\boldsymbol{h}}^{(s-1)}(n)$. Then we perform IDFT on $\boldsymbol{H}^{(s)}(\cdot,n)$ to obtain $\boldsymbol{h}^{(s)}(n)$ and calculate

$$\Delta\boldsymbol{h}^{(s)}(n)=\boldsymbol{h}^{(s)}(n)-\tilde{\boldsymbol{h}}^{(s-1)}(n). \tag{7}$$

Note that in (7) we use the reconstructed CSI $\tilde{\boldsymbol{h}}^{(s-1)}(n)$, instead of the real CSI $\boldsymbol{h}^{(s-1)}(n)$, at the UE because the latter is unavailable at the BS and thus using the former as reference can avoid quantization error propagation. This treatment is borrowed from source coding such as H.263 and H.264 [12].

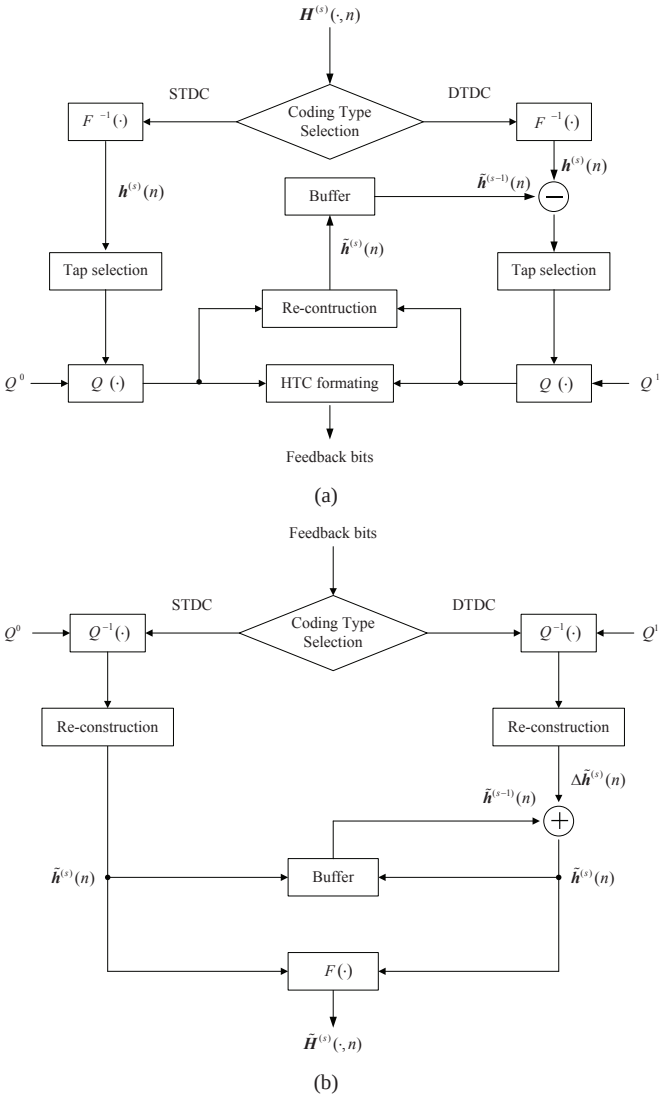

Fig. 1. Illustration diagrams of the compression (Fig. (a)) and reconstruction (Fig. (b)) processes of HTC. The functions $Q(\cdot)/Q^{-1}(\cdot)$ and $F(\cdot)/F^{-1}(\cdot)$ denote the quantization/de-quantization and DFT/IDFT processes respectively.

Afterwards, we compress $\Delta\boldsymbol{h}^{(s)}(n)$ in a similar way as that in STDC. The only difference is that the real and imaginary parts of the L^* selected taps among $\Delta\boldsymbol{h}^{(s)}(n)$ are separately quantized by another fine codebook $Q^1=\{Q_0^1,Q_1^1,\cdots,Q_{2^B-1}^1\}$.

The re-construction process for DTDC is also similar to that for STDC. Let $\Delta\tilde{\boldsymbol{h}}^{(s)}(n)$ denote the reconstructed counterpart of $\Delta\boldsymbol{h}^{(s)}(n)$. After obtaining $\Delta\tilde{\boldsymbol{h}}^{(s)}(n)$ via de-quantization, we add $\Delta\tilde{\boldsymbol{h}}^{(s)}(n)$ to $\tilde{\boldsymbol{h}}^{(s-1)}(n)$ to form the reconstructed time-domain CSI $\tilde{\boldsymbol{h}}^{(s)}(n)$. Then the corresponding frequency-domain CSI, $\tilde{\boldsymbol{H}}^{(s)}(\cdot,n)$, can be obtained by DFT.

C. Delay Index Feedback for Selected Taps

In both STDC and DTDC introduced above, the delay indexes of selected taps are necessary for the reconstruction at the BS. Denote by $\{t^{(i)}|\, i=0,1,\cdots,L^*-1\}$ the relative

positions of L^* most significant taps in $\{h^{(s)}(k^{(l)},n)|\, l = 0,1,\cdots,L-1\}$. Although we have assumed that $\{k^{(l)}|\, l = 0,1,\cdots,L-1\}$ are the same for all N links of each UE and vary every τ blocks, the amplitude of each non-zero tap is a stochastic variable and may change across every block. So are the positions of most significant taps, which therefore need to be reported every block.

One naive solution is to report the binary representation of $\{k^{(l)}|\, l = t^{(0)},t^{(1)},\cdots,t^{(L^*-1)}\}$ every block directly. However, it will cause increased feedback overhead. An ingenious alternative is as follows. From the fact that $\{k^{(l)}|\, l = t^{(0)},t^{(1)},\cdots,t^{(L^*-1)}\}$ form a subset of $\{k^{(l)}|\, l = 0,1,\cdots,L-1\}$, one can report the latter to the BS every τ blocks. The former are then reported every block by indicating their relative positions in the latter. Due to the slow variation speed assumption of $\{k^{(l)}|\, l = 0,1,\cdots,L-1\}$, τ is much larger than 1. Therefore, the overhead is dramatically reduced.

Our approach is a slightly modified version of the second solution that can further reduce the feedback overhead. Firstly, we feed back the delay indexes of all L non-zero taps every τ blocks. Then based on the observation that the power mainly concentrates on the front taps statistically, the first $C(C < L^*)$ non-zero taps, i.e., $\{k^{(l)}|\, l = 0,1,\cdots,C-1\}$ are always selected and compressed every block. Consequently, the delay index information of these C taps is known at the BS and no longer fed back. The other L^*-C taps are selected to be the most significant ones among the remaining $L-C$ non-zero taps. The delay information of these L^*-C selected taps are then reported using a binary representation that indicates their relative positions in $\{k^{(l)}|\, l = C,C+1,\cdots,L-1\}$. Note that due to this modification, the selected L^* taps may not be the most significant ones. This may lead to certain performance degradation. However, later in Section VI we will show by numerical results that, after careful parameter selection, the resultant performance degradation can be marginal.

D. Coding Type Selection

In the implementation of HTC, the selection between STDC and DTDC depends on the channel variation speed. DTDC has a higher compression efficiency than STDC in slow-varying channels and vice versa. This selection decision made at the UE side can be informed to the BS using one bit feedback. From the practical consideration that the CSI feedback mechanism is usually employed in closed-loop MIMO and the channel variation status does not change very fast, this one-bit selection decision can be fed back every τ blocks. That is, every τ blocks the UE need to process both STDC and DTDC and compare their fidelities. Afterwards, the same coding type will be adopted in the following $\tau-1$ blocks.

E. A Brief Summary

The overall process of HTC is summarized as follows. At the very beginning when the buffer is empty, STDC is assumed by default. Afterwards, the UE processes STDC or DTDC and re-selects the coding type every τ blocks. The type with a higher compression efficiency is selected and adopted in the following $\tau-1$ blocks. The compressed CSI are reported to the BS and the most recently available $\tilde{\boldsymbol{h}}^{(s)}(n)$ is stored in the buffer at the UE as the reference of future CSI compression.

V. Performance Analyses

Since TDC can be treated as a special case of STDC with $L^* = L$, a better trade-off between overhead and distortion can be achieved in the latter after parameter optimization. In addition, when the channel varies slowly, the difference between the CSI of adjacent OFDM symbols has a smaller dynamic range than the CSI itself and so DTDC can further outperform STDC. Hence we can qualitatively conclude that the HTC must have better performance than TDC. In this section, we will study the overhead-distortion performance of HTC. These analytical results are useful in the parameter optimization in the next section.

A. Overhead Analysis

Based on the discussion in the previous section, the feedback overhead of HTC per block for each UE can be calculated as

$$1/\tau + N \cdot L^* \cdot 2B + k_{\text{index}}. \tag{8}$$

In (8), the first term is contributed by the one-bit coding type selection indicator, which is fed back every τ blocks, the second term is contributed by the quantization results of L^* selected taps of all N antenna links where each tap requires $2B$ bits, and the third term, k_{index}, is contributed by the delay indexes feedback of all selected taps, which is detailed as follows.

The calculation of k_{index} is two-fold. First, the delay indexes of all L non-zero taps, $\{k^{(l)}|l = 0,1,\cdots,L-1\}$, are fed back every τ blocks. Without loss of generality, we assume $0 = k^{(0)} < k^{(1)} < \cdots < k^{(L-1)}$. Note that in practical systems, cyclic prefix (CP) is always adopted to avoid interference among adjacent OFDM symbols, indicating that the length of CP, denoted by $k_{\max}\Delta t$, is a natural upper bound for the maximum time delay of all non-zero taps. Hence we have $k^{(L-1)} \le k_{\max}$. Furthermore, we can prove $k^{(l-1)}+1 \le k^{(l)} \le k_{\max}-L+l$ holds through the following derivations. From the assumption of $0 = k^{(0)} < k^{(1)} < \cdots < k^{(L-1)} \le k_{\max}$, the left inequality holds. The right inequality can be proved by contradiction as follows. Suppose that $k^{(l)} > k_{\max}-L+l$. Then we can conclude that $k^{(l+1)} > k_{\max}-L+l+1, k^{(l+2)} > k_{\max}-L+l+2,\cdots,k^{(L-1)} > k_{\max}$, which conflicts with our assumption of $k^{(L-1)} \le k_{\max}$. Consequently, $k^{(l)}$ must be no larger than $k_{\max}-L+l$, i.e., the right inequality holds.

Obviously, $k^{(l)}$ ranging from $k^{(l-1)}+1$ to $k_{\max}-L+l$ has $k_{\max}-L+l-k^{(l-1)}$ possible values. Recall that the delay index of the first non-zero tap is assumed to be 0, i.e., $k^{(0)}=0$, and is known at both the UE and BS. Therefore $k^{(0)}$ is no longer required to be reported. The delay indexes of the other $L-1$ non-zero taps have totally $\prod_{l=1}^{L-1}\left(k_{\max}-L+l-k^{(l-1)}\right)$ possibilities. To represent these possibilities using binary number, $\left\lceil \log_2\left(\prod_{l=1}^{L-1}\left(k_{\max}-L+l-k^{(l-1)}\right)\right)\right\rceil = \left\lceil \sum_{l=1}^{L-1}\log_2(k_{\max}-L+l-k^{(l-1)})\right\rceil$ bits are required, where

$\lceil\cdot\rceil$ denotes the ceiling function. Thus we can conclude that the average number of bits used to represent all these L delay indexes should be

$$k_{\text{index}}^{(1)} = \mathop{\text{E}}_{\{k^{(l)}\}}\left(\left\lceil \sum_{l=1}^{L-1} \log_2\left(k_{\max} - L + l - k^{(l-1)}\right)\right\rceil\right). \quad (9)$$

Second, UE reports the relative indexes of $L^* - C$ selected taps among $\{k^{(l)}|l = C, C+1, \cdots, L-1\}$ for each antenna link. Without loss of generality, we also assume that the relative positions of the selected taps are stored in an ascending order, i.e., $0 \le t^{(0)} < t^{(1)} < \cdots < t^{(L^*-1)} \le L-1$. Similar to the above proof of $k^{(l-1)}+1 \le k^{(l)} \le k_{\max}-L+l$, we can easily prove that $t^{(i-1)} + 1 \le t^{(i)} \le L - L^* + i$ holds. Thus we can conclude that excluding the first C taps, the average overhead of the relative positions of the $L^* - C$ selected taps can be represented by:

$$k_{\text{index}}^{(2)} = \mathop{\text{E}}_{\{t^{(i)}\}}\left(\left\lceil \sum_{i=C}^{L^*-1} \log_2\left(L - L^* + i - t^{(i-1)}\right)\right\rceil\right) \quad (10)$$

where $t^{(-1)} = -1$. Note that (9) and (10) are achievable by bit index table lookup in the implementation and the corresponding table can be constructed using Huffman coding [18]. Combining (9) and (10), we have

$$k_{\text{index}} = k_{\text{index}}^{(1)}/\tau + N \cdot k_{\text{index}}^{(2)}. \quad (11)$$

Further substituting (11) into (8), we can obtain the average feedback overhead every block of HTC for each UE. It is worth to note that, when $L^* = L$, the term $k_{index}^{(2)}$ is equal to zero and (8) also gives the average overhead of conventional TDC when the first term $1/\tau$ is excluded.

B. Distortion Analysis

In this paper, the distortion measure for both TDC and HTC is defined as the normalized mean square error (NMSE), i.e.,

$$\begin{aligned}\sigma_e^2 =& \frac{1}{NK}\mathop{\text{E}}_{s}\left(\left\|\boldsymbol{H}^{(s)} - \tilde{\boldsymbol{H}}^{(s)}\right\|_F^2\right)\\ =& \frac{1}{NK}\sum_{n=1}^{N}\mathop{\text{E}}_{s}\left(\left\|\boldsymbol{H}^{(s)}(\cdot,n) - \tilde{\boldsymbol{H}}^{(s)}(\cdot,n)\right\|_F^2\right)\end{aligned} \quad (12)$$

where $\|\cdot\|_F$ denotes the Frobenius norm.

Firstly, recall that all $\{\boldsymbol{H}^{(s)}(\cdot,n)\}$ are i.i.d., and so are all $\{\tilde{\boldsymbol{H}}^{(s)}(\cdot,n)\}$. Then (12) can be rewritten as

$$\sigma_e^2 = \frac{1}{K}\mathop{\text{E}}_{s}\left(\left\|\boldsymbol{H}^{(s)}(\cdot,0) - \tilde{\boldsymbol{H}}^{(s)}(\cdot,0)\right\|_F^2\right) \quad (13)$$

where we only focus on the first antenna link, i.e., $n = 0$, without loss of generality.

Secondly, according to (2), we have

$$\begin{aligned}\sigma_e^2 =& \frac{1}{K}\mathop{\text{E}}_{s}\left(\left\|\boldsymbol{F}\cdot\boldsymbol{h}^{(s)}(0) - \boldsymbol{F}\cdot\tilde{\boldsymbol{h}}^{(s)}(0)\right\|_F^2\right)\\ \overset{(a)}{=}& \mathop{\text{E}}_{s}\left(\left\|\boldsymbol{h}^{(s)}(0) - \tilde{\boldsymbol{h}}^{(s)}(0)\right\|_F^2\right)\\ \overset{(b)}{=}& \mathop{\text{E}}_{s}\left(\sum_{l=0}^{L-1}\left|h^{(s)}(k^{(l)},0) - \tilde{h}^{(s)}(k^{(l)},0)\right|^2\right)\end{aligned} \quad (14)$$

where (a) follows Parseval's theorem [19] and (b) follows the fact that $\boldsymbol{h}^{(s)}(0)$ (and $\tilde{\boldsymbol{h}}^{(s)}(0)$) only contains L non-zero taps.

Thirdly, since the real and imaginary parts of each non-zero tap, i.e., $h^{(s)}(k^{(l)},0)$, are identically distributed and processed, their corresponding quantization errors have the same statistical properties (e.g., mean and variance). Hence (14) further reduces to

$$\begin{aligned}\sigma_e^2 =& 2\mathop{\text{E}}_{s}\left(\sum_{l=0}^{L-1}\left(\Re(h^{(s)}(k^{(l)},0)) - \Re(\tilde{h}^{(s)}(k^{(l)},0))\right)^2\right)\\ =& 2\mathop{\text{E}}_{s}\left(\sum_{l=0}^{L-1}\left(r^{(s)}(k^{(l)}) - \tilde{r}^{(s)}(k^{(l)})\right)^2\right)\end{aligned} \quad (15)$$

where $r^{(s)}(k^{(l)}) = \Re(h^{(s)}(k^{(l)},0))$, $\tilde{r}^{(s)}(k^{(l)}) = \Re(\tilde{h}^{(s)}(k^{(l)},0))$ and $\Re(\cdot)$ denotes the real part of its argument.

Based on (15), the distortion expressions of STDC and DTDC can then be calculated separately, as detailed below.

Distortion of STDC: Since the selected L^* taps are assumed to be the first C non-zero taps together with the $L^* - C$ most significant taps among the other $L - C$ non-zero ones. The resultant distortion can be upper bounded by that when the first L^* non-zero taps are constantly selected for compression, regardless of their relative significance. Then (15) can be rewritten as

$$\begin{aligned}\sigma_e^2 \le 2\Bigg(&\sum_{l=0}^{L^*-1}\mathop{\text{E}}_{s}\left(\left(r^{(s)}(k^{(l)}) - \tilde{r}^{(s)}(k^{(l)})\right)^2\right)\\ &+ \sum_{l=L^*}^{L-1}\mathop{\text{E}}_{s}\left(\left(r^{(s)}(k^{(l)})\right)^2\right)\Bigg)\end{aligned} \quad (16)$$

where the equality holds when $L^* = L$. Note that in (16) we have assumed $\tilde{r}^{(s)}(k^{(l)}) = 0$ for all $L^* \le l \le L-1$.

The subsequent distortion analysis for STDC relies on the the design of quantization codebook Q^0. In a practical system, Q^0 can be optimized, e.g., by Lloyd algorithm [15]. For simplicity, here we consider the simple uniform quantization in Q^0. Denote by d_0 the quantization step of codebook Q^0. Then the quantization levels in Q^0 can then be represented as $\{\pm d_0/2, \pm 3d_0/2, \cdots, \pm(2^B-1)d_0/2\}$. Hence we have

$$\begin{aligned}&\mathop{\text{E}}_{s}\left(r^{(s)}(k^{(l)}) - \tilde{r}^{(s)}(k^{(l)})\right)^2\\ &= 2\int_{(2^{B-1}-1)d_0}^{+\infty}\left(t - (2^B-1)\cdot\frac{d_0}{2}\right)^2 f(t)dt\\ &+ \sum_{i=2}^{2^B-1}\int_{(i-1-2^{B-1})d_0}^{(i-2^{B-1})d_0}\left(t - (i-1/2-2^{B-1})d_0\right)^2 f(t)dt\end{aligned} \quad (17)$$

where $f(t) = \frac{1}{\sigma_l\sqrt{\pi}}e^{-t^2/\sigma_l^2}$ is the probability density function of a Gaussian random variable t with mean zero and variance $\sigma_l^2/2$. After some derivations, (17) can be further rewritten as

$$\mathop{\text{E}}_{s}\left(r^{(s)}(k^{(l)}) - \tilde{r}^{(s)}(k^{(l)})\right)^2 \triangleq \alpha^{(l)}(B,d_0) = \sum_{i=1}^{6}\alpha_i^{(l)}(B,d_0) \quad (18)$$

where

$$\alpha_1^{(l)}(B,d_0)=\sum_{i=1}^{2^B}\frac{\sigma_l(2^B-2i)d_0}{4\sqrt{\pi}}e^{\frac{-(i-1-2^{B-1})^2d_0^2}{\sigma_l^2}},$$

$$\alpha_2^{(l)}(B,d_0)=-\sum_{i=1}^{2^B}\frac{\sigma_l(2^B+2-2i)d_0}{4\sqrt{\pi}}e^{\frac{-(i-2^{B-1})^2d_0^2}{\sigma_l^2}},$$

$$\alpha_3^{(l)}(B,d_0)=\sum_{i=1}^{2^B}\frac{\sigma_l^2+2(i-1/2-2^{B-1})^2d_0^2}{4}\mathrm{erfc}\left(\frac{(i-1-2^{B-1})d_0}{\sigma_l}\right)$$

$$\alpha_4^{(l)}(B,d_0)=-\sum_{i=1}^{2^B}\frac{\sigma_l^2+2(i-1/2-2^{B-1})^2d_0^2}{4}\mathrm{erfc}\left(\frac{(i-2^{B-1})d_0}{\sigma_l}\right),$$

$$\alpha_5^{(l)}(B,d_0)=\frac{\sigma_l(2-2^B)d_0}{2\sqrt{\pi}}e^{\frac{-2^{2B-2}d_0^2}{\sigma_l^2}},$$

$$\alpha_6^{(l)}(B,d_0)=\frac{(2^B-1)^2d_0^2+2\sigma_l^2}{4}\mathrm{erfc}\left(\frac{2^Bd_0}{2\sigma_l}\right)$$

and $\mathrm{erfc}(x)=\frac{2}{\sqrt{\pi}}\int_x^\infty e^{-t^2}dt$ is the complementary error function. The derivation for (18) is given in Appendix B.

From (16) and (18), we obtain an upper bound for the distortion of STDC as

$$\sigma_e^2\le 2\left(\sum_{l=0}^{L^*-1}\alpha^{(l)}(B,d_0)+\sum_{l=L^*}^{L-1}\frac{\sigma_l^2}{2}\right). \tag{19}$$

Note that (19) holds with equality when $L=L^*$, which exactly quantifies the distortion performance of TDC.

Distortion of DTDC: A similar upper bound for the distortion performance of DTDC can be obtained by assuming the residual of the first L^* taps are selected for compression. Specifically, we have $\tilde{r}^{(s)}(k^{(l)})=\tilde{r}^{(s-1)}(k^{(l)})$ for all $L^*\le l\le L-1$ and (15) is rewritten as

$$\begin{aligned}\sigma_e^2&\le 2\left(\begin{array}{l}\sum_{l=0}^{L^*-1}\mathop{\mathrm{E}}_s\left(r^{(s)}(k^{(l)})-\tilde{r}^{(s)}(k^{(l)})\right)^2\\+\sum_{l=L^*}^{L-1}\mathop{\mathrm{E}}_s\left(r^{(s)}(k^{(l)})-\tilde{r}^{(s-1)}(k^{(l)})\right)^2\end{array}\right)\\&\overset{(a)}{=}2\left(\begin{array}{l}\sum_{l=0}^{L^*-1}\mathop{\mathrm{E}}_s\left(r^{(s)}(k^{(l)})-\tilde{r}^{(s)}(k^{(l)})\right)^2\\+\sum_{l=L^*}^{L-1}\mathop{\mathrm{E}}_s\left(r^{(s-1)}(k^{(l)})-\tilde{r}^{(s-1)}(k^{(l)})\right)^2\\+\sum_{l=L^*}^{L-1}\mathop{\mathrm{E}}_s\left(r^{(s)}(k^{(l)})-r^{(s-1)}(k^{(l)})\right)^2\end{array}\right)\\&=2\left(\begin{array}{l}\sum_{l=0}^{L-1}\mathop{\mathrm{E}}_s\left(r^{(s)}(k^{(l)})-\tilde{r}^{(s)}(k^{(l)})\right)^2\\+\sum_{l=L^*}^{L-1}\mathop{\mathrm{E}}_s\left(r^{(s)}(k^{(l)})-r^{(s-1)}(k^{(l)})\right)^2\end{array}\right)\end{aligned} \tag{20}$$

where (a) follows the independence between the quantized error of previous CSI and the current CSI change in the time domain, i.e., $r^{(s-1)}(k^{(l)})-\tilde{r}^{(s-1)}(k^{(l)})$ is independent of $r^{(s)}(k^{(l)})-r^{(s-1)}(k^{(l)})$. The two terms in (20) will be derived separately below.

Similar to the treatment of Q^0, we assume Q^1 to be a uniform quantization codebook as well. We further assume $d_0=A\cdot d_1$. For the derivation of the first term in (20), we will reuse the counterpart result derived in STDC by converting DTDC to STDC with more quantization steps equivalently. The following lemma gives the necessary and sufficient conditions on A which guarantee the fidelity of the above conversion. Its proof is given in Appendix C.

Lemma 1: When the previous CSI is quantized by STDC, if and only if $A=\{1,2,\cdots,2^{B-1}\}$, the quantization effect of the current CSI by DTDC using $d_1=\frac{1}{A}d_0$ is the same as that by STDC using an equivalent codebook, denoted by Q^2, with $\left(A\cdot 2^B+2^B-A\right)$ quantization levels and step $d_2=d_1$.

Furthermore, in the design of the quantization step, the statistic properties of the quantized object should be taken into account. Specifically, the quantization step should be proportionate to the root of the variance of the quantized object. Thus, A should be given by

$$\begin{aligned}A&=\frac{\sqrt{\mathop{\mathrm{E}}_s\left(r^{(s)}\left(k^{(l)}\right)\right)^2}}{\sqrt{\mathop{\mathrm{E}}_s\left(r^{(s)}\left(k^{(l)}\right)-\tilde{r}^{(s-1)}\left(k^{(l)}\right)\right)^2}}\\&\overset{(a)}{=}\frac{\sqrt{\mathop{\mathrm{E}}_s\left(r^{(s)}\left(k^{(l)}\right)\right)^2}}{\sqrt{\mathop{\mathrm{E}}_s\left(r^{(s)}\left(k^{(l)}\right)-r^{(s-1)}\left(k^{(l)}\right)\right)^2+\mathop{\mathrm{E}}_s\left(r^{(s-1)}\left(k^{(l)}\right)-\tilde{r}^{(s-1)}\left(k^{(l)}\right)\right)^2}}\end{aligned} \tag{21}$$

where (a) follows the independence between the quantized error of previous CSI and the current CSI change in time domain. Note that in the implementation, the quantization step is usually small, indicating that the second term in the dominator of (21) is always much smaller than the first term. Here we omit the second term and A can be therefore approximated to

$$A\approx\frac{\sqrt{\mathop{\mathrm{E}}_s\left(r^{(s)}\left(k^{(l)}\right)\right)^2}}{\sqrt{\mathop{\mathrm{E}}_s\left(r^{(s)}\left(k^{(l)}\right)-r^{(s-1)}\left(k^{(l)}\right)\right)^2}} \tag{22}$$

where the numerator is clearly $\frac{\sigma_l}{\sqrt{2}}$, and the expectation in the denominator of (22) can be written as:

$$\begin{aligned}&\mathop{\mathrm{E}}_s\left(r^{(s)}\left(k^{(l)}\right)-r^{(s-1)}\left(k^{(l)}\right)\right)^2\\&=\mathop{\mathrm{E}}_s\left(\rho\cdot r^{(s-1)}\left(k^{(l)}\right)+\sqrt{1-\rho^2}\cdot\Re\left(\xi^{(s)}\left(k^{(l)},0\right)\right)-r^{(s-1)}\left(k^{(l)}\right)\right)^2\\&\overset{(a)}{=}\mathop{\mathrm{E}}_s\left((\rho-1)\cdot r^{(s-1)}\left(k^{(l)}\right)\right)^2+\mathop{\mathrm{E}}_s\left(\sqrt{1-\rho^2}\cdot\Re\left(\xi^{(s)}\left(k^{(l)},0\right)\right)\right)^2\\&\overset{(b)}{=}(\rho-1)^2\cdot\frac{\sigma_l^2}{2}+(1-\rho^2)\cdot\frac{\sigma_l^2}{2}\\&=(1-\rho)\sigma_l^2.\end{aligned} \tag{23}$$

In (23), the equalities (a) and (b) follow the assumptions that $\xi^{(s)}\left(k^{(l)},0\right)$ and $h^{(s)}\left(k^{(l)},0\right)$ are independent and identically distributed, respectively.

Thus (22) can be rewritten as

$$A \approx \frac{1}{\sqrt{2-2\rho}}. \quad (24)$$

Combining Lemma 1 and (24), $\tilde{r}^{(s)}(k^{(l)})$ can be regarded as the quantization result of $r^{(s)}(k^{(l)})$ by directly using STDC with an equivalent uniform codebook containing quantization levels $\{\pm d_1/2, \pm 3d_1/2, \cdots, \pm q_{\max} d_1/2\}$ where[2] $q_{\max}=(A+1)\cdot(2^B-1)$ and $A=\min\left(\max\left(1, \left\lfloor \frac{1}{\sqrt{2-2\rho}} \right\rfloor\right), 2^{B-1}\right)$ and the floor function $\lfloor\cdot\rfloor$ is to compensate the effect caused by the approximation process taken in (22), i.e., $\mathop{\mathrm{E}}_{s}\left(r^{(s-1)}\left(k^{(l)}\right)-\tilde{r}^{(s-1)}\left(k^{(l)}\right)\right)^2=0$. Hence by replacing d_0 and (2^B-1) with d_1 and $q_{\max}$ in (18), we obtain

$$\mathop{\mathrm{E}}_{s}\left(r^{(s)}(k^{(l)})-\tilde{r}^{(s)}(k^{(l)})\right)^2 \le \alpha^{(l)}(\log_2(q_{\max}+1), d_1). \quad (25)$$

The derivation for the second term in (20) can be easily obtained from (23) as

$$\mathop{\mathrm{E}}_{s}\left(r^{(s)}\left(k^{(l)}\right)-r^{(s-1)}\left(k^{(l)}\right)\right)^2=(1-\rho)\sigma_l^2. \quad (26)$$

Combining (20), (25) and (26), we can upper bound the distortion of DTDC as

$$\sigma_e^2 \le 2\left(\sum_{l=0}^{L^*-1}\alpha^{(l)}\left(\log_2\left(q_{\max}+1\right), d_1\right)+\sum_{l=L^*-1}^{L-1}(1-\rho)\sigma_l^2\right). \quad (27)$$

VI. System Level Simulation Results

In this section, we study the performance of the proposed HTC scheme in the real environments via the system level simulations. Our simulation settings typically consist of multiple cells and UEs and account for system attributes including scheduling and HARQ. The parameters used in our simulation follow the guidelines of 3GPP Case 1 (see Table A.2.1.1-1/2 in [17]) which involve typical parameters for the simulation under the macro-only homogeneous deployment. Specifically, the carrier frequency is 2GHz and the system bandwidth is 10MHz. The network topology consists of 19 sites, where each site has 3 hexagonal shaped cells. Each cell is covered by one BS, which is assumed to be equipped with 4 transmit antennas, i.e., $N=4$. The cells' inter site distance (ISD) is set to 500 meters. The total transmit power of each BS is 46dBm, i.e., 40w. Within each cell coverage area, 10 single-antenna UEs are independently generated and uniformly distributed. The channel coefficients between each UE-and-BS pair are generated according to the spatial channel model (SCM) [14]. The SCM model is developed particularly for system level evaluation by standardization bodies (3GPP-3GPP2). SCM considers $L=6$ clusters of scatterers, where each cluster corresponds to a non-zero tap. The generation of the channel coefficient of each tap consists of three basic steps [14]: specifying scenario, obtaining the parameters associated with the corresponding scenario and generating the channel coefficients based on the parameters. In our simulation, the scenario of urban macro is adopted. Please refer to [14] for detailed introduction of SCM generation procedure.

[2]Here $q_{\max}$ is obtained assuming that the CSI at the $(s-1)$-th block is compressed by STDC. Actually, if DTDC is adopted instead at the $(s-1)$-th block, the resultant maximum quantization level can be larger than $q_{\max}d_1/2$ and corresponding distortion can be even less.

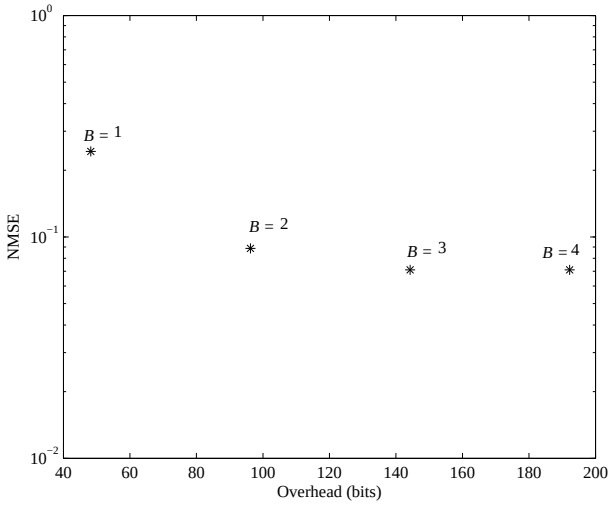

Fig. 2. Overhead-distortion performance of TDC for the quantization books' payload of B =1, 2, 3 and 4.

A. Parameter Optimization

We first optimize the parameters of both TDC and HTC. Through the Monte Carlo method, we obtain the PDP of $(0.3290, 0.2513, 0.2024, 0.1623, 0.0488, 0.0062)$ and $\rho=0.9$ for SCM statistically.

For TDC, we scale B from 1 to 4 and calculate the corresponding overhead-distortion performance using (8) and (19). As shown in Fig. 2, TDC achieves the best trade-off at $B=2$. Further increasing the payload of codebook only brings marginal performance improvement at the cost of much heavier feedback overhead. In what follows, the TDC performance with $B=2$ (the corresponding overhead is 96.24bits averagely) is adopted as the baseline for HTC.

Next we optimize the parameters (L^*, B, C) for HTC subject to the constraint that HTC has no higher overhead than TDC. Recalling from the discussion in Section V-B, we can see that the obtained distortion upper bounds (19) and (27) are independent of the parameter C. Therefore, we first fix $C=0$ in the overhead calculation and optimize (L^*, B) for both STDC and DTDC based on (8), (19) and (27), respectively. The optimized parameters are exhaustively searched from all settings that satisfy the overhead constraint. The corresponding overhead-distortion performance of both STDC and DTDC are shown in Fig. 3, from which we can see that the setting $(L^*=5, B=2)$ minimizes the distortions of STDC and DTDC at the same time.

Given the setting $(L^*=5, B=2)$, we further optimize the parameter C using the overhead calculated by (8) and the distortion obtained by the Monte Carlo method. As shown in Fig. 4, a significant overhead reduction can be observed when C increases, but an additional distortion to the reconstructed CSI is also incurred meanwhile. However when $C \le 2$ in STDC and $C \le 4$ in DTDC, the accuracy degradation is marginal and

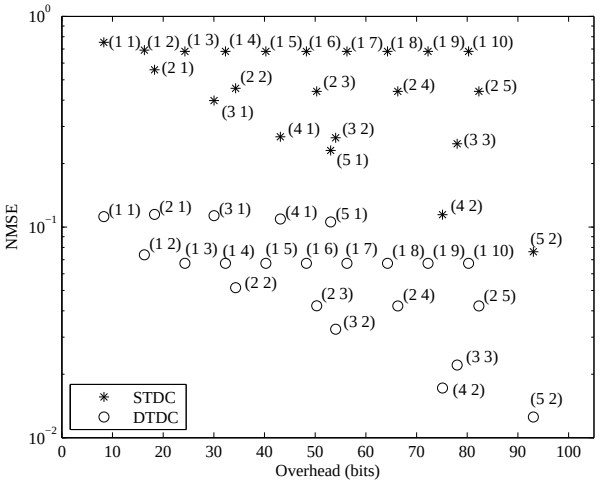

Fig. 3. Overhead-distortion performance of HTC under various parameters L^* and B. The parameter settings (L^* B) are marked on the points.

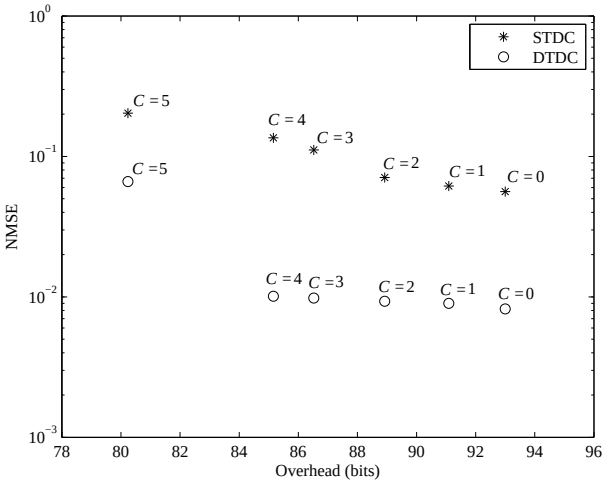

Fig. 4. Overhead-distortion performance of HTC with $L^* = 5$, $B = 2$, and C is 0, 1, 2, 3, 4, and 5 respectively.

better overhead-distortion trade-off can be achieved. Hence the optimized parameter settings are $(L^* = 5, B = 2, C = 2)$ for STDC and $(L^* = 5, B = 2, C = 4)$ for DTDC. It is also seen that, in the considered SCM model, DTDC significantly outperforms STDC. Hence in our simulation, DTDC dominates the HTC performance.

B. Simulation Results

We now provide some simulation examples to illustrate the potential gains achieved by adopting HTC in various transmission strategies.

The workflow in the simulation is as follows. By the current LTE-A standard, each BS first broadcasts one common reference signal (CRS) continuously. The CRSs from different cells are assumed to be mutually orthogonal at each UE. Each UE then measures the received power of the CRSs[3] from different BSs and selects the BS offering the highest CRS power as its serving BS. Afterwards, the CSI between each UE and its serving BS is estimated and compressed at the UE side using parameter-optimized TDC or HTC. In our simulation, we assume perfect CSI estimation at the UE side so as to exclude the impact of channel estimation on the system performance. Upon receiving the compressed CSI fed back from UEs, each BS then perform scheduling among its served UEs based on their reconstructed CSI. Specifically, the 10 MHz system bandwidth is divided into 10 sub-bands. On each sub-band, the serving BS schedules either a single UE or multiple UEs based on the well-known proportional fair (PF) principle. We refer to the former as single-user MIMO (SU-MIMO) and the latter as multi-user MIMO (MU-MIMO) in this paper for the definition clarification. After scheduling, the serving BS selects proper modulation and coding scheme (MCS) levels and beamforming vectors for the served UEs. In particular, the beamforming vectors are computed based on the maximum eigenmode beamforming (MEB) [1] and the zeroforcing beamforming (ZFBF) strategy for SU-MIMO and MU-MIMO, respectively. During the transmitting process, the major radio resource management (RRM) algorithms such as packet scheduling, closed-loop MIMO with precoding, link adaption, and HARQ, are also implemented.

Fig. 5 shows the cumulative distribution functions (CDFs) of the throughputs per UE achieved by different CSI compression schemes under SU-MIMO MEB and MU-MIMO ZFBF. The performance obtained by adopting ideal reconstructed CSI at the serving BS is also plotted as an upper bound. It can be seen from Fig. 5 that the gaps between the throughputs obtained by adopting TDC and the upper bound are significant, especially in MU-MIMO ZFBF. Contrarily when HTC is adopted in the system, the corresponding performance gaps become marginal for both SU-MIMO MEB and MU-MIMO ZFBF. In particular, compared to the performance obtained by TDC in SU-MIMO MEB, a gain of 14.68% is achieved by HTC at the cell average throughput and a gain of 22.00% at the 5% quantiles [17] (denoted by 5%-ile below) worst UE throughput, where 5%-ile is obtained at the 5% point of the CDF curve and indicates the cell-edge performance. In MU-MIMO ZFBF, the counterpart gains are 64.62% and 33.33%. Thus we can conclude that HTC outperforms TDC [9] completely.

It is worth to note that the performance of HTC can be further improved by optimizing the quantization books via Lloyd method [15]. Numerically, we find that the advantage of quantization book optimization is more significant in MU-MIMO ZFBF than in SU-MIMO MEB. This is because MU-MIMO ZFBF is more sensitive to the inaccuracy of CSI at the BS. Even though, we find through simulation that the performance improvement of HTC after quantization book optimization is very limited, e.g., a gain of 6.24% at the cell average throughput and a gain of 10.08% at the 5%-ile worst UE throughput in MU-MIMO ZFBF. This implies that HTC is insensitive to the quantization codebook.

VII. Realization Issues

Finally, we consider the realization of HTC in practice. Similar to TDC, the DFT/IDFT operations involved in HTC

[3]In LTE-A, the metrics of the received power of the CRSs is referred to as reference signal received power (RSRP)

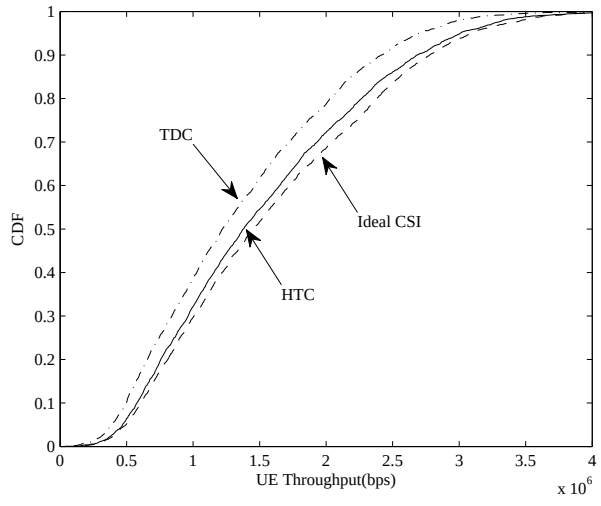

(a)

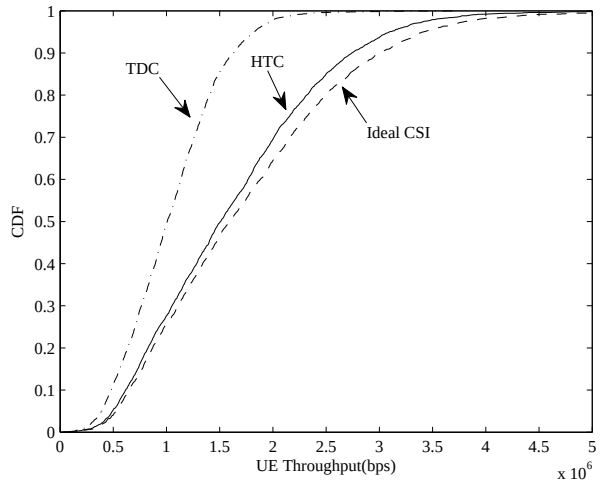

(b)

Fig. 5. Comparison of the system level performance for different feedback schemes assuming SU-MIMO MEB (Fig. (a)) and MU-MIMO ZFBF (Fig. (b)).

are inherent operations in OFDM systems and have fast implementation algorithms with very low computational cost, and a quantization codebook at the UE as well as the BS only incurs very limited space complexity. Moreover, HTC involves the following additional complexity:

- subtraction in (7) for computing the residual $\Delta \boldsymbol{h}^{(s)}(n)$;
- comparison for finding the most significant taps of each link;
- additional buffer to store the reconstructed CSI and two index mapping table to achieve (9) and (10).

The abovementioned additional operations involve very low computational cost. The additional buffer is required to just store several scalars. Hence the implementation complexity of HTC is similar to that of TDC. Note that although an additional codebook for DTDC, i.e., Q^1, is required in HTC, it can be generated by properly scaling the quantization steps of Q^0 in the practical implementation according to the dynamic range of the difference between adjacent CSI. Hence it is unnecessary to store Q^1 in the buffer.

VIII. Conclusions

In this paper, we have developed a novel compression and feedback scheme, i.e., HTC, for the CSI of downlink MIMO-OFDM systems. HTC has the capability of exploiting the correlation of CSI in both frequency and time domains. Its performance is evaluated both analytically and experimentally. First the closed-form expressions are developed for the overhead of these two coding types. Then the parameters involved in HTC are optimized based on the analytical results. Finally, under LTE-A Release 10 based cellular networks, the system level performance of HTC is evaluated and compared with that of TDC in both MEB based SU-MIMO and ZFBF based MU-MIMO. Both the overhead-distortion performance analysis and the system level simulations demonstrate that HTC can significantly outperform the available alternative and achieve very high compression efficiency.

Although we have assumed independent CSI for different BS antennas in the paper, the HTC scheme can be directly applied to the system where the BS antennas are correlated due to close deployment. It is expected that, by improving the current HTC scheme to further explore the correlation in the spatial domain, even higher CSI compression efficiency can be achieved. This interesting topic is currently under investigation.

Appendix A
Proof of Theorem 1

Treating $\boldsymbol{H}_m^{(s)}(\cdot, n)$ as a time-domain signal and according to Nyquist sampling theorem, we can see that the sampling frequency (denoted by f_s) should be at least twice the highest frequency contained in $\boldsymbol{H}_m^{(s)}(\cdot, n)$ (denoted by f_c) so as to avoid distortion, i.e.,

$$f_s = \frac{K^*}{T_s} \geq 2 f_c \tag{28}$$

where T_s denotes the periodicity of one OFDM symbol.

By IDFT, the signal $\boldsymbol{H}_m^{(s)}(\cdot, n)$ can be transformed into $\boldsymbol{h}_m^{(s)}(n)$. Since we have treated $\boldsymbol{H}_m^{(s)}(\cdot, n)$ as a time-domain signal, $\boldsymbol{h}_m^{(s)}(n)$ can then be regarded as the frequency-domain spectrum of $\boldsymbol{H}_m^{(s)}(\cdot, n)$. Thus the bandwidth of each subcarrier in $\boldsymbol{h}_m^{(s)}(n)$ is $1/T_s$. We assume $\boldsymbol{h}_m^{(s)}(n)$ contains L non-zero subcarriers. Thus the highest frequency f_c is lower bounded by L/T_s, i.e.,

$$f_c \geq \frac{L}{T_s}. \tag{29}$$

Note that (29) holds with equality only when the front L subcarriers in $\boldsymbol{h}_m^{(s)}(n)$ are non-zero. Comparing (28) and (29), we can obtain

$$K^* \geq 2L. \tag{30}$$

This completes the proof.

APPENDIX B
THE DERIVATIONS FROM (17) TO (18)

The first term in (17) can be rewritten as

$$\begin{aligned}
&2\int_{(2^{B-1}-1)d_0}^{+\infty}\left(t-(2^B-1)\cdot\frac{d_0}{2}\right)^2 f(t)dt\\
=&2\int_{(2^{B-1}-1)d_0}^{2^{B-1}d_0}\left(t-(2^B-1)\frac{d_0}{2}\right)^2 f(t)dt+2\int_{2^{B-1}d_0}^{+\infty}\left(t-(2^B-1)\frac{d_0}{2}\right)^2 f(t)dt\\
=&\int_{-(2^{B-1}-1)d_0}^{-2^{B-1}d_0}\left(t+(2^B-1)\frac{d_0}{2}\right)^2 f(t)dt+2\int_{2^{B-1}d_0}^{+\infty}\left(t-(2^B-1)\frac{d_0}{2}\right)^2 f(t)dt\\
&+\int_{(2^{B-1}-1)d_0}^{2^{B-1}d_0}\left(t-(2^B-1)\cdot\frac{d_0}{2}\right)^2 f(t)dt. \qquad (31)
\end{aligned}$$

Substituting (31) into equation (17) of our paper, we obtain

$$\begin{aligned}
&\mathop{\mathrm{E}}_{s}\left(r^{(s)}(k^{(l)})-\tilde{r}^{(s)}(k^{(l)})\right)^2=\\
&\sum_{i=1}^{2^B}\int_{(i-1-2^{B-1})d_0}^{(i-2^{B-1})d_0}\left(t-(i-1/2-2^{B-1})d_0\right)^2 f(t)dt\\
&+2\int_{2^{B-1}d_0}^{+\infty}\left(t-(2^B-1)\cdot\frac{d_0}{2}\right)^2 f(t)dt. \qquad (32)
\end{aligned}$$

For notational simplicity, we define $T=2^B$, $R=\frac{Td_0}{2}=2^{B-1}d_0$, $x_i=id_0-R=(i-2^{B-1})d_0$, $y_i=\frac{x_{i-1}+x_i}{2}=\left(i-1/2-2^{B-1}\right)d_0$, and $y_T=\frac{x_{T-1}+x_T}{2}=\left(2^{B-1}-1/2\right)d_0$. Recalling that $f(t)=\frac{1}{\sigma_l\sqrt{\pi}}e^{-\frac{t^2}{\sigma_l^2}}$, we can rewrite (32) as

$$\begin{aligned}
&\mathop{\mathrm{E}}_{s}\left(r^{(s)}(k^{(l)})-\tilde{r}^{(s)}(k^{(l)})\right)^2\\
=&\sum_{i=1}^{T}\int_{x_{i-1}}^{x_i}(t-y_i)^2 f(t)dt+2\int_{R}^{+\infty}(t-y_T)^2 f(t)dt\\
=&\sum_{i=1}^{T}\int_{x_{i-1}}^{x_i}t^2 f(t)dt+\sum_{i=1}^{T}\int_{x_{i-1}}^{x_i}-2ty_i f(t)dt+\sum_{i=1}^{T}\int_{x_{i-1}}^{x_i}y_i^2 f(t)dt\\
&+2\int_{R}^{+\infty}t^2 f(t)dt+2\int_{R}^{+\infty}-2ty_T f(t)dt+2\int_{R}^{+\infty}y_T^2 f(t)dt\\
=&\underbrace{\sum_{i=1}^{T}\int_{x_{i-1}}^{x_i}\frac{t^2}{\sigma_l\sqrt{\pi}}e^{-\frac{t^2}{\sigma_l^2}}dt}_{(a)}+\underbrace{\sum_{i=1}^{T}\int_{x_{i-1}}^{x_i}\frac{-2y_i t}{\sigma_l\sqrt{\pi}}e^{-\frac{t^2}{\sigma_l^2}}dt}_{(b)}\\
&+\underbrace{\sum_{i=1}^{T}\int_{x_{i-1}}^{x_i}\frac{{y_i}^2}{\sigma_l\sqrt{\pi}}e^{-\frac{t^2}{\sigma_l^2}}dt}_{(c)}+\underbrace{2\int_{R}^{+\infty}\frac{t^2}{\sigma_l\sqrt{\pi}}e^{-\frac{t^2}{\sigma_l^2}}dt}_{(d)}\\
&\underbrace{+2\int_{R}^{+\infty}\frac{-2y_T t}{\sigma_l\sqrt{\pi}}e^{-\frac{t^2}{\sigma_l^2}}dt}_{(e)}+\underbrace{2\int_{R}^{+\infty}\frac{y_T^2}{\sigma_l\sqrt{\pi}}e^{-\frac{t^2}{\sigma_l^2}}dt}_{(f)}. \qquad (33)
\end{aligned}$$

The above six terms are separately derived as follows. First, after integration by parts, terms (a) and (d) can be rewritten as

$$\begin{aligned}
(a)&=\sum_{i=1}^{T}\left(-\frac{\sigma_l t}{2\sqrt{\pi}}e^{-\frac{t^2}{\sigma_l^2}}\Big|_{x_{i-1}}^{x_i}+\int_{x_{i-1}}^{x_i}\frac{\sigma_l}{2\sqrt{\pi}}e^{-\frac{t^2}{\sigma_l^2}}dt\right)\\
&=\sum_{i=1}^{T}\left(\frac{\sigma_l x_{i-1}}{2\sqrt{\pi}}e^{-\frac{x_{i-1}^2}{\sigma_l^2}}-\frac{\sigma_l x_i}{2\sqrt{\pi}}e^{-\frac{{x_i}^2}{\sigma_l^2}}\right)\\
&\quad+\sum_{i=1}^{T}\left(\frac{\sigma_l^2}{4}\mathrm{erfc}\left(\frac{x_{i-1}}{\sigma_l}\right)-\frac{\sigma_l^2}{4}\mathrm{erfc}\left(\frac{x_i}{\sigma_l}\right)\right), \qquad (34)\\
(d)&=-\frac{\sigma_l t}{\sqrt{\pi}}e^{-\frac{t^2}{\sigma_l^2}}\Big|_{R}^{+\infty}+\int_{R}^{+\infty}\frac{\sigma_l}{\sqrt{\pi}}e^{-\frac{t^2}{\sigma_l^2}}dt\\
&=\frac{\sigma_l R}{\sqrt{\pi}}e^{-\frac{R^2}{\sigma_l^2}}+\frac{\sigma_l^2}{2}\mathrm{erfc}\left(\frac{R}{\sigma_l}\right). \qquad (35)
\end{aligned}$$

Second, by integration, terms (b) and (e) can be rewritten as

$$(b)=\sum_{i=1}^{T}\frac{\sigma_l y_i}{\sqrt{\pi}}e^{-\frac{t^2}{\sigma_l^2}}\Big|_{x_{i-1}}^{x_i}=\sum_{i=1}^{T}\left(\frac{\sigma_l y_i}{\sqrt{\pi}}e^{-\frac{{x_i}^2}{\sigma_l^2}}-\frac{\sigma_l y_i}{\sqrt{\pi}}e^{-\frac{{x_{i-1}}^2}{\sigma_l^2}}\right), \qquad (36)$$

$$(e)=\frac{2\sigma_l y_T}{\sqrt{\pi}}e^{-\frac{t^2}{\sigma_l^2}}\Big|_{R}^{+\infty}=\frac{-2\sigma_l y_T}{\sqrt{\pi}}e^{-\frac{R^2}{\sigma_l^2}}. \qquad (37)$$

Third, terms (c) and (f) can be represented by the complementary error function, i.e., $\mathrm{erfc}(x)=\frac{2}{\sqrt{\pi}}\int_{x}^{+\infty}e^{-t^2}dt$, as

$$\begin{aligned}
(c)&=\sum_{i=1}^{T}\left(\frac{{y_i}^2}{\sqrt{\pi}}\int_{x_{i-1}}^{+\infty}e^{-\left(\frac{t}{\sigma_l}\right)^2}d\left(\frac{t}{\sigma_l}\right)-\frac{{y_i}^2}{\sqrt{\pi}}\int_{x_i}^{+\infty}e^{-\left(\frac{t}{\sigma_l}\right)^2}d\left(\frac{t}{\sigma_l}\right)\right)\\
&=\sum_{i=1}^{T}\left(\frac{{y_i}^2}{2}\mathrm{erfc}\left(\frac{x_{i-1}}{\sigma_l}\right)-\frac{{y_i}^2}{2}\mathrm{erfc}\left(\frac{x_i}{\sigma_l}\right)\right), \qquad (38)\\
(f)&=y_T^2\frac{2}{\sqrt{\pi}}\int_{R}^{+\infty}e^{-\left(\frac{t}{\sigma_l}\right)^2}d\left(\frac{t}{\sigma_l}\right)=y_T^2\mathrm{erfc}\left(\frac{R}{\sigma_l}\right). \qquad (39)
\end{aligned}$$

Combining (34)–(39), we have

$$\begin{aligned}
&\mathop{\mathrm{E}}_{s}\left(r^{(s)}(k^{(l)})-\tilde{r}^{(s)}(k^{(l)})\right)^2\\
&\sum_{i=1}^{T}\left(-\frac{\sigma_l t}{2\sqrt{\pi}}e^{-\frac{t^2}{\sigma_l^2}}\Big|_{x_{i-1}}^{x_i}+\int_{x_{i-1}}^{x_i}\frac{\sigma_l}{2\sqrt{\pi}}e^{-\frac{t^2}{\sigma_l^2}}dt\right)\\
&=\sum_{i=1}^{T}\left(\frac{\sigma_l x_{i-1}}{2\sqrt{\pi}}e^{-\frac{x_{i-1}^2}{\sigma_l^2}}-\frac{\sigma_l x_i}{2\sqrt{\pi}}e^{-\frac{{x_i}^2}{\sigma_l^2}}\right)\\
&+\sum_{i=1}^{T}\left(\frac{\sigma_l^2}{4}\mathrm{erfc}\left(\frac{x_{i-1}}{\sigma_l}\right)-\frac{\sigma_l^2}{4}\mathrm{erfc}\left(\frac{x_i}{\sigma_l}\right)\right)
\end{aligned}$$

$$
\begin{aligned}
&+\sum_{i=1}^{T}\left(\frac{\sigma_l y_i}{\sqrt{\pi}}e^{-\frac{{x_i}^2}{\sigma_l^2}}-\frac{\sigma_l y_i}{\sqrt{\pi}}e^{-\frac{{x_{i-1}}^2}{\sigma_l^2}}\right)\\
&+\sum_{i=1}^{T}\left(\frac{{y_i}^2}{2}\mathrm{erfc}\left(\frac{x_{i-1}}{\sigma_l}\right)-\frac{{y_i}^2}{2}\mathrm{erfc}\left(\frac{x_i}{\sigma_l}\right)\right)\\
&+\frac{\sigma_l R}{\sqrt{\pi}}e^{-\frac{R^2}{\sigma_l^2}}+\frac{\sigma_l^2}{2}\mathrm{erfc}\left(\frac{R}{\sigma_l}\right)-\frac{2\sigma_l y_T}{\sqrt{\pi}}e^{-\frac{R^2}{\sigma_l^2}}+y_T^2\mathrm{erfc}\left(\frac{R}{\sigma_l}\right)\\
&=\sum_{i=1}^{T}\left(\begin{array}{l}\left(\frac{x_{i-1}}{2}-y_i\right)\frac{\sigma_l}{\sqrt{\pi}}e^{-\frac{x_{i-1}^2}{\sigma_l^2}}-\left(\frac{x_i}{2}-y_i\right)\frac{\sigma_l}{\sqrt{\pi}}e^{-\frac{{x_i}^2}{\sigma_l^2}}\\ +\frac{\sigma_l^2+2{y_i}^2}{4}\mathrm{erfc}\left(\frac{x_{i-1}}{\sigma_l}\right)-\frac{\sigma_l^2+2{y_i}^2}{4}\mathrm{erfc}\left(\frac{x_i}{\sigma_l}\right)\end{array}\right)\\
&+(R-2y_T)\frac{\sigma_l}{\sqrt{\pi}}e^{-\frac{R^2}{\sigma_l^2}}+\frac{\sigma_l^2+2y_T^2}{2}\mathrm{erfc}\left(\frac{A}{\sigma_l}\right). \qquad (40)
\end{aligned}
$$

Finally, by replacing T, R, x_i, y_i and y_T with their definitions and after combining like terms, (40) can be further rewritten as

$$
\begin{aligned}
&\mathop{\mathrm{E}}_{s}\left(r^{(s)}(k^{(l)})-\tilde{r}^{(s)}(k^{(l)})\right)^2\\
&=\sum_{i=1}^{2^B}\frac{\sigma_l\left(2^B-2i\right)d_0}{4\sqrt{\pi}}e^{\frac{-\left(i-1-2^{B-1}\right)^2d_0^2}{\sigma_l^2}}\\
&-\sum_{i=1}^{2^B}\frac{\sigma_l\left(2^B+2-2i\right)d_0}{4\sqrt{\pi}}e^{\frac{-(i-2^{B-1})^2d_0^2}{\sigma_l^2}}\\
&+\sum_{i=1}^{2^B}\frac{\sigma_l^2+2\left(i-1/2-2^{B-1}\right)^2d_0^2}{4}\mathrm{erfc}\left(\frac{\left(i-1-2^{B-1}\right)d_0}{\sigma_l}\right)\\
&-\sum_{i=1}^{2^B}\frac{\sigma_l^2+2\left(i-1/2-2^{B-1}\right)^2d_0^2}{4}\mathrm{erfc}\left(\frac{(i-2^{B-1})d_0}{\sigma_l}\right)\\
&+\frac{\sigma_l(2-2^B)d_0}{2\sqrt{\pi}}e^{-\frac{2^{2B-2}d_0^2}{\sigma_l^2}}+\frac{\left(2^B-1\right)^2d_0^2+2\sigma_l^2}{4}\mathrm{erfc}\left(\frac{2^Bd_0}{2\sigma_l}\right), \qquad (41)
\end{aligned}
$$

which is the same as (18).

APPENDIX C
PROOF OF LEMMA 1

The rationale behind Lemma 1 is two-fold, as detailed below.

1) The equivalent quantization codebook Q^2 should be uniform

This is equivalent to say that, when we spread all the quantization levels of Q^1 around two adjacent quantization levels of Q^0, the resultant two quantization ranges[4] should be overlapped with an integer number of d_1. Without loss of generality, let us consider the quantization levels $-\frac{d_0}{2}$ and $\frac{d_0}{2}$ of Q^0. Mathematically, we have

$$-\frac{d_0}{2}+2^{B-1}d_1=\frac{d_0}{2}-2^{B-1}d_1+nd_1, \qquad (42)$$

for some integer n, $n=0,1,2,\cdots,2^B-1$, or equivalently

$$A=\frac{d_0}{d_1}=2^B-n, \qquad (43)$$

for some integer n, $n=0,1,2,\cdots 2^B-1$. Hence all the feasible values of A that guarantees Q^2 to be uniform are $\{1,2,\cdots,2^B\}$.

2) The overflowing event should be avoided

If the value of A is improperly selected, it is possible that when DTDC is selected after coding type selection, the corresponding $\Delta r^{(s)}(k^{(l)})$ is out of the quantization range of Q^1. Under this situation, the quantization results by using DTDC with codebook Q^1 will be different from those by using STDC with codebook Q^2 and thus the equivalence between them does not hold.

To avoid such an event, we need carefully choose the value of A such that once $\Delta r^{(1)}(k^{(l)})$ is out of the quantization range of Q^1, DTDC always leads to a larger distortion than STDC and will not be selected for compression. Without loss of generality, we assume that the previous quantized level by STDC is $\tilde{r}^{(0)}(k^{(l)})=-\frac{d_0}{2}$. Mathematically, it is equivalent to let

$$-\frac{d_0}{2}+\frac{2^B-1}{2}d_1\le\frac{2n-1}{2}d_0\le-\frac{d_0}{2}+\frac{2^B+1}{2}d_1, \qquad (44)$$

for some integer n, $n=1,2,\cdots,2^{B-1}$, or equivalently

$$\frac{2^B-1}{2n}\le\frac{d_0}{d_1}=A\le\frac{2^B+1}{2n}, \qquad (45)$$

for some integer n, $n=1,2,\cdots,2^{B-1}$. Therefore, we can conclude that the feasible values of A that avoid the above overflowing event are $\{1,2,\cdots,2^{B-1}\}$.

In summary, when the previous CSI is quantized by STDC, if and only if $A=\{1,2,\cdots,2^{B-1}\}$, the quantization effect of the current CSI by DTDC using $d_1=\frac{1}{A}d_0$ is the same as that by STDC using the equivalent codebook Q^2.

[4]When we spread all quantization levels of Q^1 around a point x, the resultant quantization range is defined as $\left[x-2^{B-1}d_1,x+2^{B-1}d_1\right]$. It is easy to see that for all the terms falling within this quantization range, the corresponding quantization error is always no larger than $d_1/2$

REFERENCES

[1] P. Wang, and P. Li, "On maximum eigenmode beamforming and multi-user gain," *IEEE Trans. on Inf. Theory*, vol. 57, no. 7, pp. 4170-4180, Jul. 2011.

[2] M. Chiani, M. Z. Win, and H. Shin, "MIMO networks: the effects of interference," *IEEE Trans. on Inf. Theory*, vol. 56, no.1, pp. 336-349, Jan. 2010.

[3] I. Sarris, and A. R. Nix, "Design and performance assessment of high-capacity MIMO architectures in the presence of a line of sight component," *IEEE Trans. Veh. Technol.*, vol. 56, no. 4, pp. 2194-2202, Jul. 2007.

[4] P. Xia, S. Zhou, and G. B. Giannakis, "Adaptive MIMO-OFDM based on partial channel state information," *IEEE Trans. Sig. Proc.*, vol. 52, no.1, pp. 202-213, Jun. 2004.

[5] N. Jindal, "MIMO broadcast channels with finite rate feedback," *IEEE Trans. Inform. Theory*, vol. 52, no. 11, pp. 5045-5059, Nov. 2006.

[6] G. Caire, N. Jindal, M. Kobayashi, and N. Ravindran, "Multiuser MIMO achievable rates with downlink training and channel state feedback," *IEEE Trans. Inf. Theory*, vol. 56, no. 6, pp. 2845-2866, Jun. 2010.

[7] F. Wang, A. Ghosh, C. B. Sankaran, P. J. Fleming, F. Hsieh, and S. J. Benes, "Mobile WiMAX systems: performance and evolution," *IEEE Commun. Mag.*, vol. 22, no. 10, pp. 41-49, Oct. 2008.

[8] A. Ghosh, R. Ratasuk, B. Mondal, N. Mangalvedhe, T. A. Thomas, "LTE-advanced: next-generation wireless broadband technology," *IEEE Wireless Commun.*, vol. 17, no. 3, pp. 10-22, Jun. 2010.

[9] H. Shirani-Mehr, and G. Caire, "Channel state feedback schemes for multiuser MIMO-OFDM downlink," *IEEE Trans. Commun.*, vol. 57, no. 9, pp.2713-2723, Sept. 2009.
[10] K. E. Baddour and N. C. Beaulieu, "Autoregressive models for fading channel simulation," *in Proc. IEEE GlobeCom*, Nov. 2001.
[11] G. W. Peters, I. Nevat, and J. Yuan, "Channel estimation in OFDM systems with unknown power delay profile using transdimensional MCMC," *IEEE Trans. Signal Processing*, vol. 57, no.9, pp. 3545-3561. Sept. 2009.
[12] G. J. Sullivan, and T. Wiegand, "Video compression-from concepts to the H.264/AVC standard," *Proceedings of the IEEE*, vol. 93, no.1, Jan. 2005.
[13] Y. P. Zhang, P. Wang, Q. Li, and P. Zhang, "Hybrid transform coding for channel state information in MIMO-OFDM systems," *in Proc. IEEE Int. Conf. Commun.*, Kyoto, Japan, Jun. 2011.
[14] "Technical specification group radio access network; spatial channel model for Multiple Input Multiple Output (MIMO) simulations," *3GPP TR 25.996 V. 8.0.0*, Dec. 2008. Available at: ftp://ftp.3gpp.org/Specs/latest/Rel-8/25_series/.
[15] S. P. Lloyd, "Least Squares Quantization in PCM," *IEEE Trans. on Inf. Theory*, vol. IT-28, pp. 129-137, Mar. 1982.
[16] "Evolved Universal Terrestrial Radio Access (E-UTRA); User Equipment (UE) radio transmission and reception," *3GPP TS 36.101 V. 8.5.1*, Mar. 2009. Available at: ftp://ftp.3gpp.org/Specs/2009-03/Rel-8/36_series/.
[17] "Evolved Universal Terrestrial Radio Access (E-UTRA); Further advancements for E-UTRA physical layer aspects," *3GPP TR 36.814 V. 9.0.0*, Mar. 2010. Available at: ftp://ftp.3gpp.org/Specs/2010-03/Rel-9/36_series/.
[18] D. A. Huffman, "A method for the construction of minimum-redundancy codes," *Proceedings of the I.R.E.*, vol. 40, no. 9, pp. 1098-1102, Sept. 1952.
[19] P. Z. Peebles, *Probability, Random Variables and Random Signal Principles*. New York: McGraw-Hill, 1993.

Yong-Ping Zhang (M'11) received the B.Eng. degree in telecommunication engineering and M.Eng. degree (with the highest honor) in pattern recognition and intelligent systems from Xidian University, China, in 2001 and 2004, respectively. He is currently a visiting scholar in the department of Electrical Engineering at Stanford University. He is also with the Research Department of HiSilicon, Huawei Technologies as a senior research engineer. Prior to joining Huawei in 2006, he was with China Telecom Shenzhen Branch as a program engineer and with Ricoh Software Research Center Beijing (SRCB) as a research engineer. His current research interests are MIMO techniques and inter-cell interference management for Heterogeneous Networks.

PLACE PHOTO HERE

Peng Wang (S'05-M'10) received received the B.Eng. and M.Eng. degrees in telecommunication engineering from Xidian University, China, in 2001 and 2004,respectively, and the Ph.D. degree in electronic engineering from the City University of Hong Kong, Hong Kong SAR, in 2010. He was a Research Fellow with the City University of Hong Kong and a visiting Post-Doctor Research Fellow with the Chinese University of Hong Kong, Hong Kong SAR, both from 2010 to 2012. He is currently a Research Fellow with the University of Sydney, Australia. His research interests include channel and network coding, iterative multi-user detection, MIMO techniques and millimetre-wave communications.

Shulan Feng (M'10) received the B.S and M.S degrees from Harbin Institue of Technologies, Harbin, China in 1997 and 1999 respectively. She joined Huawei Technologies Co. LTD in 2000. Currently, she is involved in the research of 5G wireless communication. Her research interests include CR/SDR, device-to-device communication and MIMO.

PLACE PHOTO HERE

Philipp Zhang (Chen-Xiong Zhang) (M' 86) was born in Shanghai, China. He received the B.S. degree in electrical engineering from Shanghai Jiao-Tong University, China, and the M.S. and Ph.D. degrees in electrical engineering from the University of Karlsruhe, Germany.

In 1983, he joined the Institute for Theoretical Electrical Engineering at the University of Karlsruhe, where he was involved in teaching and research activities in VLSI layout and circuit design, and high-speed analog and digital mixed chip design. From 1991 to 1995, he was with SIEMENS Microelectronic Center, Hamburg, Germany, where he was involved in research and development of ATM broadband networks and ASIC design for telecom application. He was involved in the R&D of Advanced Communication technologies in Europe (RACE) project. In 1995 he transferred to Interphase Corp., Dallas, TX. He was Technical Director and responsible for the development of chipsets for broadband/optical communication systems. After then he has worked in a couple of start-up high-tech companies as founder/CTO/CEO. In these companies, he was responsible for the strategic technical directions for the companies and R&D management in the area circuit design and ASIC/SoC/RF chips for digital TV/video, wireless networks and broadband communication. In 2005, he joined Hisilicon/Huawei Technologies as Chief Scientist and is currently in charge of corporate research programs/projects.

Dr. Zhang holds a number of German patents. He published books and many technical papers. His seminar on MPEG over Broadband Networks took place in many countries on behalf of standa rd organizations. He received two RACE Awards from the European Union RACE program commissioner for "extraordinary contribution and outstanding application/demonstration in 1995. He also received the Best Paper Award at the 1991 IEEE IJCNN in Singapore, and an Outstanding Research Activity Award from the state of Baden-Wuertemberg, Germany.

PLACE PHOTO HERE

Sheng Tong received the Ph.D. degree from Xidian University, Xi'an, China, in 2006. He was a Lecturer with Xidian University from 2006 to 2011 and a Research Fellow with City University of Hong Kong from 2007 to 2009. He is currently a lecturer with University of Wollongong, Australia, and an Associate Professor with Xidian University, China. His research interests include channel coding and iterative receiver design in digital communication systems.